Mon. Not. R. Astron. Soc. **000**, 000–000 (0000) Printed 1 February 2008 (MN LATEX style file v2.2)

Periodic photometric variability of the brown dwarf Kelu-1

F.J. Clarke[1], C.G. Tinney[2] and K.R. Covey[3]
[1] *Institute of Astronomy, Madingley Road, Cambridge CB3 0HA, UK.*
[2] *Anglo-Australian Observatory, Epping, Australia.*
[3] *Carleton College, MN, USA.*
email: fclarke@ast.cam.ac.uk, cgt@aaoepp.aao.gov.au

1 February 2008

ABSTRACT
We have detected a strong periodicity of 1.80±0.05 hours in photometric observations of the brown dwarf Kelu-1. The peak-to-peak amplitude of the variation is ∼1.1% (11.9±0.8 mmag) in a 41nm wide filter centred on 857nm and including the dust/temperature sensitive TiO & CrH bands. We have identified two plausible causes of variability: surface features rotating into- and out-of-view and so modulating the light curve at the rotation period; or, elliposidal variability caused by an orbiting companion. In the first scenario, we combine the observed $v \sin i$ of Kelu-1 and standard model radius to determine that the axis of rotation is inclined at 65±12° to the line of sight.

Key words: Stars: brown dwarfs – Stars: oscillations – Stars: rotation – Stars: atmospheres – Binaries: close

1 INTRODUCTION

The study of rotation and variability in main sequence stars has led to a great improvement in our understanding of their physics (e.g. Stauffer & Hartmann 1986). Recently, several groups have shown that variability can also be detected in substellar brown dwarfs (Tinney & Tolley 1999; Bailer-Jones & Mundt 1999, 2001; Martín, Zapatero Osorio & Lehto 2001).

In this paper we present differential photometry of the brown dwarf Kelu-1, in a search for rotational variability. Kelu-1 is a field brown dwarf, discovered by Ruiz, Leggett & Allard (1997) via its large proper motion. It is classified as an L2 dwarf in the scheme of Kirkpatrick et al. (2000), and model fits to its spectrum estimate an effective temperature of 1900±100K (Ruiz et al. 1997). The parallax distance of 19.6±0.5 pc gives an absolute magnitude of M_J=11.96±0.09 (Kirkpatrick et al. 2000) or a bolometric magnitude of M_{bol}=13.9±0.1. The detection of strong lithium absorption (Ruiz et al. 1997) in an object of this luminosity implies a mass below 0.07$M_\odot$ (Tinney 1998), making Kelu-1 a bona fide brown dwarf. In common with many L- and M-type brown dwarfs (Basri et al. 2000, Tinney & Reid 1998), Kelu-1 is a very rapid rotator with a measured $v \sin i$=60±5 kms^{-1}. It is thought this may indicate that the magnetic braking mechanisms which operate in more massive stars do not operate with the same efficiency in brown dwarfs (as first suggested by Tinney & Reid 1998).

In section 2 we describe the data acquisition and reduction. Time series analysis of the resulting differential photometry is presented in section 3. In section 4 we discuss our observations in terms of surface features on the brown dwarf, or the nature of an orbiting companion.

2 DATA

2.1 Observations

Kelu-1 was observed on 2000 March 24-25 using the Taurus-2 instrument on the 3.9m Anglo-Australian Telescope with a CCD detector denoted MITLL3. MITLL3 is a 2096×4096 pixel device with 15μm pixels, giving an image scale of 0.373" per pixel. Observations were performed through an intermediate bandpass blocking filter for the Taurus Tunable Filter. This filter (denoted R6) is 41nm wide and is centred at 858nm. The bandpass of the filter is shown overlaid on a spectrum of Kelu-1 (taken from Martín et al. 1999) in Figure 1. Also plotted in Figure 1 is the spectrum of the slightly hotter L0 dwarf DENIS-P J0909-0658 (Martín et al. 1999), indicating the temperature sensitivity of the TiO and CrH molecular bandheads selected by our filter.

A specially constructed slot mask was installed in the focal plane wheel of Taurus-2 (the same mask used by Tinney & Tolley 1999). Multiple exposures of a sky field can then be made through this slot, between which charge is shuffled and stored on the unilluminated surface of the CCD. When used to observe Kelu-1, the entire Taurus-2 instrument was rotated at an angle of 140°, so that several suitable photometric reference stars could be observed (see Figure 2). This

Table 1. Log of Kelu-1 observations in March 2000.

Date	Start UT	End UT	# Images	Exposure Time (s)
24^{th}	11:20	11:53	60	60
24^{th}	13:15	14:00	90	30
24^{th}	15:04	19:05	480	30
25^{th}	10:10	12:56	270	30
25^{th}	13:39	19:00	300	60

Figure 1. The spectrum of Kelu-1 (solid line) compared with the spectrum of the L0 (slightly hotter) brown dwarf DENIS-P J0909-0658 (dashed line). The transmission profile of the R6 filter is overplotted (dot-dash line), showing how it isolates the sensitive TiO and CrH features at ∼850nm.

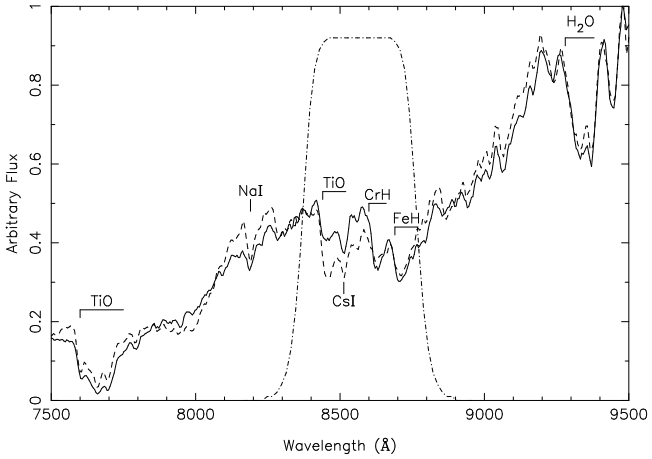

observing technique results in a series of 30 exposures, following which the CCD is read out only once, providing very low read-out overheads and precise timing. Table 1 gives a log of the observations.

2.2 Reduction and photometry

Each CCD frame contains 30 seperate exposures, so the data processing is slightly more complicated than for standard CCD imaging. Each *frame* was bias subtracted and then sliced into thirty individual *exposures*. The header file for each *exposure* was modified so as to include the correct timing and positional information. A master flatfield *exposure* was then constructed from dome flats observed in the same manner as the data. The data were then divided by this flat, providing correction to the ∼1% level.

Due to the proximity of a nearby star to our primary target, point-spread function (PSF) photometry of this data is required. Photometry was performed using DAOPHOT within the IRAF environment. A PSF was determined for each individual exposure by fitting a profile to several of the brightest (non-saturated) stars in the field. This profile was then scaled to all the stars in the field to determine their brightness. No faint neighbours were found after the PSF had been subtracted from the target stars. Pixels which varied by more than 5% from the mean in the flatfield were flagged as bad. These bad pixels were interpolated over during the PSF fitting stage, but completely ignored during the actual photometry. PSF photometry also has the advantage of being relatively immune to cosmic ray events, which would affect aperture photometry. In order to verify our PSF photometry, we also performed aperture photometry in the same fashion as Martín et al. (2001). The aperture photometry was found to give the same, but noisier, results as the PSF photometry.

Figure 2. "Slot" mask image of Kelu-1 and the *comparison* and *check* stars used in our differential photometric analysis. The vertical bars in the image are bad columns on the MITLL3 detector. The orientation of the sky through the mask when Taurus-2 is rotated to PA=140° is indicated.

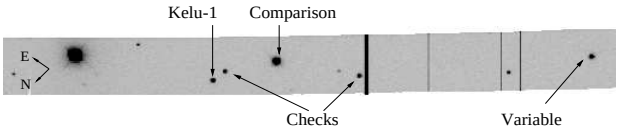

To obtain high precision differential photometry of Kelu-1, we compared its apparent brightness with that of surrounding reference stars, cancelling the effects of apparent brightness changes due to variable extinction, seeing, instrument performance or exposure time. There are four available reference stars in our field-of-view (the brightest star in the field was often saturated). We define the brightest of these four stars to be our *comparison* star, which sets the magnitude zero-point for each exposure. The three remaining stars can then be used as *check* stars, allowing us to detect intrinsic variability in our *comparison* star. One of the *check* stars was found to be variable and therefore discarded. The remaining *checks* were averaged to define a mean *check* magnitude. These stars are identified in Figure 2.

The differential lightcurves obtained are shown in Figure 3. The top panel shows Kelu-1 minus *comparison*, and the lower panel *comparison* minus *check*. It is clear from these plots that Kelu-1 minus *comparison* photometry is more variable than *comparison* minus *check* photometry - indicating the variability detected is due to changes in the apparent brightness of Kelu-1 itself (an increase in δm represents a dimming of Kelu-1). Variability in the *comparison* star would manifest itself as equal, but opposite, changes in each lightcurve. This effect can be seen on the first group of datapoints - the Kelu-1 minus *comparison* data is above the mean, and the *comparison* minus *check* photometry is below the mean, indicating the *comparison* star has dimmed. We neglect this group of (60) datapoints in further analysis.

As the photometry presented in Figure 3 is differential, most sources of systematic error which might produce a "spurious" signal in Kelu-1 are cancelled out. The remaining possible sources of error are differential effects due to the differences in colour of Kelu-1 and the reference stars, or their different locations on the CCD.

Differential position effects have been minimized by keeping all objects within 30 pixels of a nominal position on the detector for all observations. However, differential photometry for Kelu-1 versus detector position shows a residual correlation between δm and y-position on the CCD (Figure 4). We have fitted this correlation with a straight line and subtracted it. The cause of this effect remains unknown. The maximum pixel-to-pixel sensitivity variation in the flat field is 2.5% in the region of interest, and does not display any gradient. All data discussed hence have had this correlation removed. No correlation was found with x-position.

Differential colour effects will be produced when the effective wavelength of a star through a filter is different from

Figure 3. The top panel shows differential photometry for Kelu-1 (in the sense Kelu-1 minus *comparison* as described in §2.2) over two nights. The bottom panel shows *comparison* minus *check* to the same scale, clearly indicating the variability detected is from Kelu-1, not the *comparison*. The uncertainties plotted are based on the photon counting errors as produced by DAOPHOT and propagated to the differential results for Kelu-1, *comparison* and *check* stars. This plot shows raw differential photometry, before the correlation of Figure 4 is removed.

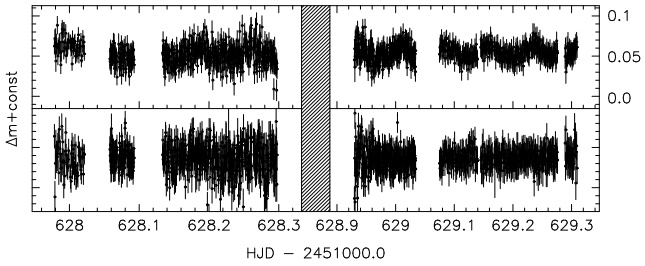

Figure 4. Differential photometry plotted against Y pixel position on the CCD. There is a clear correlation at the level of 0.003mag per pixel, which we remove by subtracting a straight line fit.

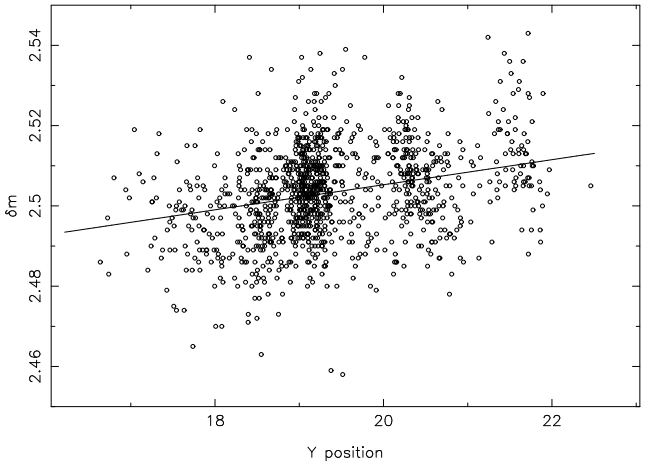

the reference objects. The target will then suffer a different amount of atmospheric extinction as the target rises and sets. If such an effect is present we would expect that spurious periodicities would be produced at aliases of 24 hours (ie 6, 12 or 24 hours). We would also expect to observe a correlation between differential photometry and airmass if this effect is present. Figure 5 shows a plot of the differential photometry for Kelu-1 (upper panel) and comparison stars (lower panel) versus airmass. There is no evidence (from Rank-Spearman tests) for a correlation in either of these plots. In addition, Figure 1 shows that Kelu-1 does not have a strong colour gradient over our filter band-pass.

3 TIME SERIES ANALYSIS

We have calculated the least-squares weighted power spectrum of the differential lightcurve to look for periodicities. The power spectrum is calculated in the manner described by Frandsen et al. (1995), which we briefly describe here. The data are represented by the function $A_i \sin(2\pi f_i t + \phi_i)$ for a range of frequencies f_i, where A_i, ϕ_i and t are the

Figure 5. Differential photometry plotted against airmass for Kelu-1 minus *comparison* (top panel) and *comparison* minus *check* (bottom panel). A Rank-Spearman correlation test shows no significant correlation between airmass and differential magnitude.

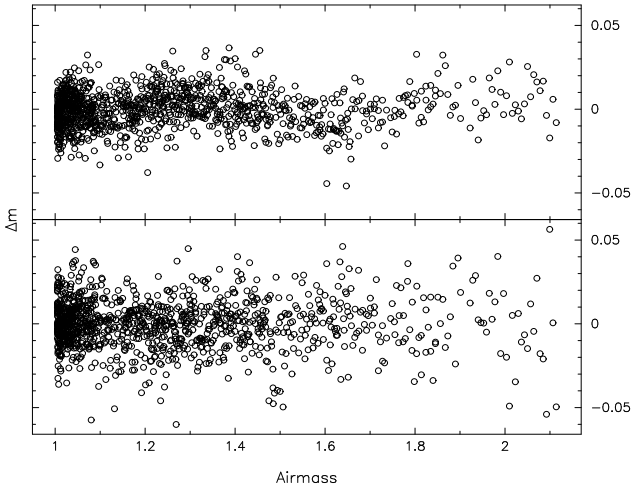

amplitude, phase and time respectively. The power at each frequency is then $P_i = A_i^2 = \alpha^2 + \beta^2$, where α and β are given by

$$\alpha = (sc_2 - cx)/(s_2c_2 - x^2),$$
$$\beta = (cs_2 - sx)/(s_2c_2 - x^2)$$

with

$$c = \sum w_j x_j \cos(\Omega_i t_j),$$
$$s = \sum w_j x_j \sin(\Omega_i t_j),$$
$$c_2 = \sum w_j \cos^2(\Omega_i t_j),$$
$$s_2 = \sum w_j \sin^2(\Omega_i t_j),$$
$$x = \sum w_j \sin(\Omega_i t_j)\cos(\Omega_i t_j)$$

where (t_j,x_j,w_j) are the data points & associated weights and $\Omega_i = 2\pi f_i$. Each data point is assigned a weight of $w_j = 1/e_j^2$, where e_j is the error associated with point j. This system gives data points with smaller errors higher weights.

The discrete sampling of observations means that the observed power spectrum is the convolution of the "true" power spectrum, with the "window function". We have calculated the window function as prescribed by Roberts et al. (1987);

$$W(f) = \frac{1}{N}\sum_j e^{-2\pi i f t_j} \quad (1)$$

The power spectrum and window function of our data are shown in Figure 6. The upper panel shows the power spectrum over the complete range of frequencies available to us; one day^{-1} up to the Nyquist frequency of 0.5 min^{-1} ($1 < f < 720$ day^{-1}; $24 > P > 0.033$ hours). There is only one main peak in the power spectrum. The lower panel shows a close-up of the region of interest ($1 < f <$

30 day^{-1}). The power spectrum of the Kelu-1 differential photometry (solid line) shows a strong peak at a frequency of 13.34±0.38 day^{-1}, corresponding to a period of 1.80±0.05 hours. The peaks at higher and lower frequencies are produced by the first sidelobes of the window function, as shown in the middle panel of Figure 6. The maximum power of the main peak is 3.5x10^{-5} mag^2, corresponding to a peak-peak amplitude in the lightcurve of 11.9 mmag. Monte-Carlo simulations of the data give a 1-σ error in the amplitude of 11.9±0.8 mmag. CLEANed power spectra (Roberts et al. 1987) do not reveal any other periodicities hiding in the sidelobes of the main frequency.

Also shown in the lower panel of Figure 6 is the power spectrum of the *comparison* minus *check* photometry (dashed line). There is no peak at the frequency detected in the Kelu-1 photometry, and the maximum power in this spectrum is an order of magnitude lower. This confirms the periodic variability we detect in the Kelu-1 minus *comparison* photometry is due to intrinsic variability of Kelu-1 rather than the *comparison* star.

To further investigate the periodicity detected, we have treated each night's data separately. The periodograms are shown in Figure 7. The same ∼1.8 hour periodicity is detected in both datasets, indicating the source of the variability is stable over at least ∼48 hours (∼25 rotations).

Close examination of the data reveals a slow linear change in Kelu-1's brightness at a level of 0.003 mag/day over the duration of the observations (this is not caused by the previously discussed correlation between δm and y-position on the CCD (Figure 4). We have *not* removed this effect for the time-series analysis. Figure 8 shows the Kelu-1 photometry folded on a period of 1.80 hours (with the slow, linear trend this time removed), and combined into 5 minute bins. We derive the following ephemeris for the time of minimum light, t_{min};

$$t_{min} = \text{JD } 2451628.037 + 0.075 \times \epsilon$$

where ϵ is the number of rotations since JD=2451628.037.

Figure 6. The lower panel shows the least-squares weighted power spectrum of Kelu-1 minus *comparison* (solid line) and *comparison* minus *check* (dashed line). There is a clear peak at 13.33 day^{-1} (period=1.80±0.05 hours) with a peak-to-peak amplitude of 11.9 mmag in the Kelu-1 power spectrum. The error bar represents the 1-σ width of the central peak. There is no corresponding peak in the *comparison* minus *check* power spectrum, showing that the detected period is from Kelu-1. The middle panel shows the window function of the dataset, clearly indicating the peak is not due to sampling effects. The upper-most panel shows the least-squares weighted power spectrum of Kelu-1 over the entire range of frequencies we can study, from 1 day^{-1} to the Nyquist frequency of 0.5 min^{-1}. This panel shows there is no significant structure in the power spectrum above f∼20 day^{-1}

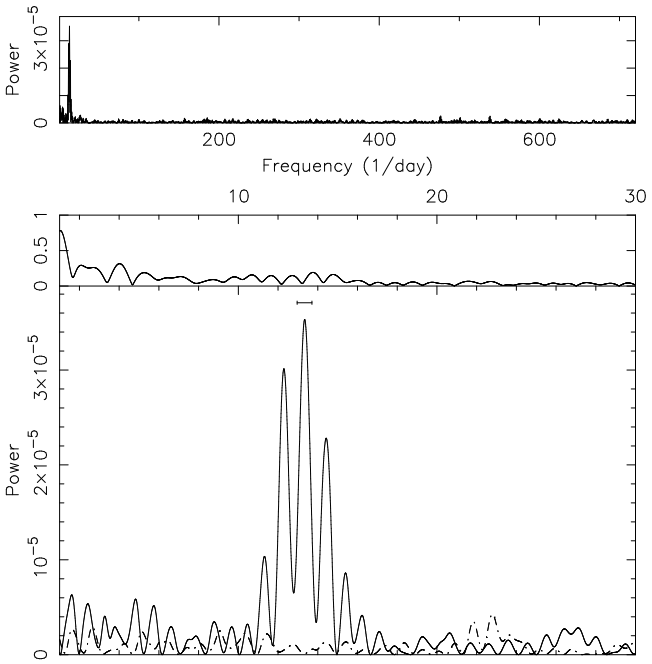

4 DISCUSSION

Kelu-1 clearly displays periodic variability, but what is the cause of this variability? We have developed four possible explanations which we discuss in this section:

(i) surface inhomegeneity moderated by meteorology and variable dust formation;
(ii) surface inhomegeneity moderated by magnetic starspots;
(iii) light curve variability due to gravitational (i.e. tidal) distortion of Kelu-1's envelope by a close companion; and
(iv) light curve variability due to an eclipsing binary.

4.1 Dust cloud meteorology

At the cool temperature of Kelu-1's photosphere, dust formation will play an important role. Theoretical spectra indicate that Kelu-1 is better matched by models with dust suspended in the photosphere than models in which condensates are "rained-out" (Baraffe et al. 1998). We cannot expect, however, the atmospheres of brown dwarfs to be placid, homogenous places — especially if rotating at $v \sin i$ =60 km s^{-1}. They are no doubt dynamic and evolving, much like the atmospheres seen on planets in our own solar system. This leads us to investigate the possibility that we are observing dust cloud meteorology in Kelu-1's atmosphere.

Gelino et al. (2001) suggest there is a possible correlation between J-K$_s$ colour and variability in L dwarfs – variable objects tend to have bluer J-K$_s$ colours, which they claim is evidence that *holes* in dust clouds are causing variability. Kelu-1 has a J-K$_s$ ∼ 1.6 (Kirkpatrick et al. 1999). This is not significantly different from the mean colour for an L2 dwarf (J-K$_s$ ∼ 1.5), so Kelu-1's strong variability sheds no light on this suggestion.

Could the variability be due to a large feature on one side of the brown dwarf? The surfaces of all the Solar System giant planets are dominated by surface banding, which is driven by an interior in which Coriolis forces dominate over buoyant convection, to produce long, thin quasi-cylindrical cells oriented with their axes parallel to the axis of rotation (Schubert & Zhang 2000). In brown dwarfs, however, – even brown dwarfs with a 1.8h rotation period – buoyancy forces should dominate to produce chaotic three dimensional convection. So banding structures, like those seen on Jupiter, are probably not to be expected. If cloud formation

Figure 7. Power spectrum of data from night 1 (upper panel) & 2 (lower panel). The same peak at $\sim$13 day^{-1} is detected in both datasets. The upper section in both panels shows the window function.

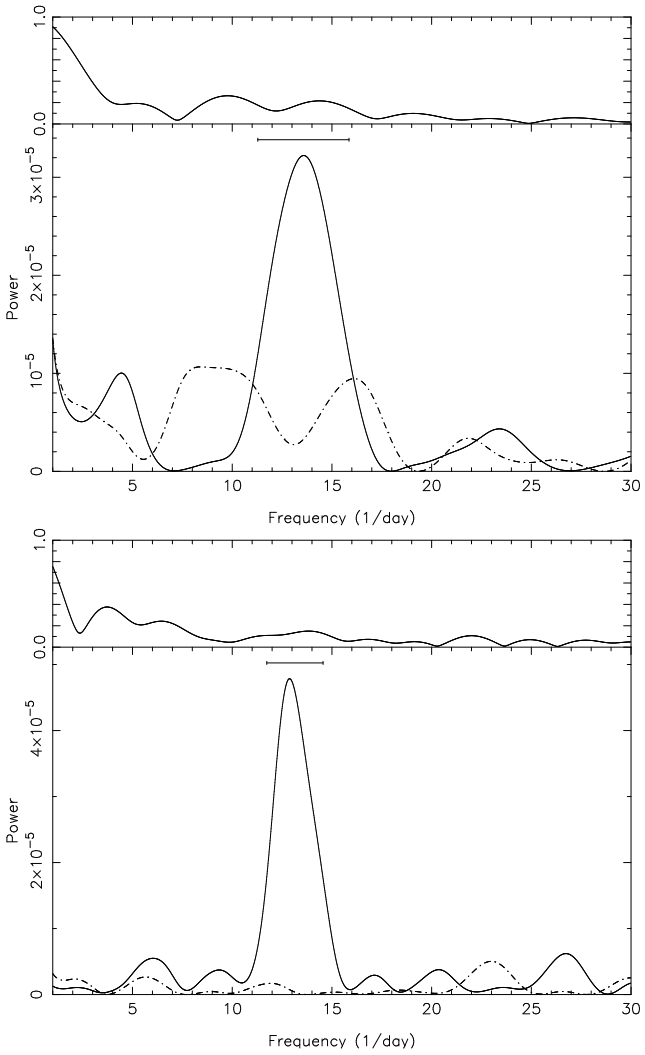

Figure 8. Kelu-1 photometry folded onto the main period (1.80 hours), and combined into 5 minute bins to improve the signal to noise ratio. This data has had a long term trend of δm brightening at $\sim$3 mmag/day removed.

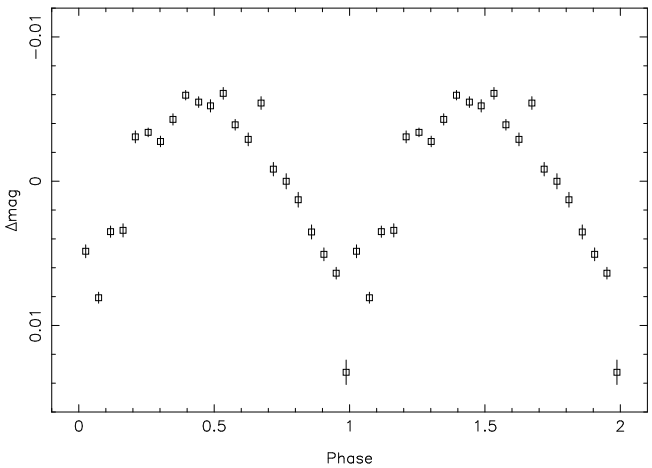

is inhomogenous, rotation and convection should combine to produce less ordered structures. So convective upwelling, or large cloud inhomogeneities may be possible.

4.2 Magnetic starspots

Another possibility is that the imhomogeneities we detect are caused by magnetically induced starspots, analogous to those observed on the Sun and other cool stars. However, Gelino et al. (2001) have shown that the atmospheres of brown dwarfs are unable to sustain starspots, as low Reynolds numbers imply the atmosphere is not bound to magnetic field lines. In addition, several groups have shown that there no strong evidence for the link between variability and activity (as measured by H-α equivelent width), which would be expected if magnetic forces drove variability. We note however that this conclusion is weakened by the small number statistics currently involved.

4.3 Binarity

One intriguing possibility is that we are seeing variability induced by a companion orbiting Kelu-1. A companion could modify Kelu-1s brightness in two ways; either by partial or total eclipsing, or via the gravitational pertubation of Kelu-1's photosphere, causing ellipsoidal variability (see Hilditch 2001). We have not been able to derive any orbital configuration which could reproduce the observed lightcurve amplitude and shape, and we therefore reject an eclipsing companion. In the case of ellipsodial variability, we would observed two maxima per rotation, and hence the orbital period would be 3.6 hours. It is reasonable to assume the orbits will be circular due to tidal effects, and we can therefore directly calculate the orbital seperation as;

$$a = 0.48 R_{\odot} \left(\frac{M_1}{0.065 M_{\odot}} \right)^{1/3} \left(\frac{P}{3.6\mathrm{h}} \right)^{2/3} \qquad (2)$$

where M_1 is the primary (Kelu-1) mass, and P is the orbital period.

Unfortunately, when fitting for ellipsodial variability, there is a degeneracy between the mass of the secondary object and the orbital inclination of the system. If, however, we assume the secondary companion is also a brown dwarf (lack of X-ray flux rejects the possibility of a massive dark companion such as a neutron star or black-hole), we can place limits on its mass. Figure 9 shows the possible secondary mass as a function of primary mass. Companions are excluded from the hatched region for two different reasons: (1) if $M_1 \geq 45 M_{\mathrm{jup}}$, the minimum mass is determined by the need to produce 1.1% ellipsodial variability without the secondary causing eclipses (i$\leq$65°), (2) for $M_1 \leq 45 M_{\mathrm{jup}}$, brown dwarfs cannot exist in the hatched region, as they would overflow their Roche-lobes, transfering matter to the primary. It is not clear what the final outcome of such an interaction would be, but the lack of activity indicates this cannot currently be happening. An object more compact than a brown dwarf or gas-giant planet could survive in this region. We note that these limits are based on simplistic models and are very sensitive to the exact amplitude of Kelu-1's variability. They do however indicate that any

Figure 9. Allowed masses for a companion to Kelu-1. If Kelu-1 has a mass greater than $\sim 45 M_{jup}$, the minimum mass limit is set by the need to induce 1.1% elliposidal variations with i$\leq$65°. However, if Kelu-1 has a mass less than $\sim 45 M_{jup}$, brown dwarfs/gas-giant planets are excluded from the hatched region as they would overflow their Roche-lobe.

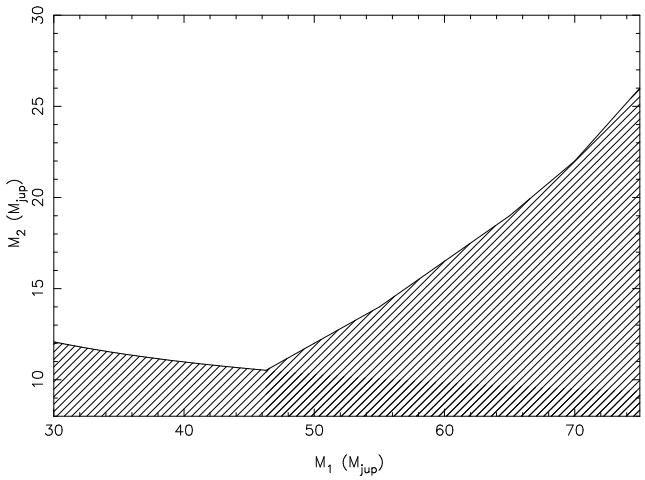

companion to Kelu-1 would be a brown dwarf rather than massive planet (i.e. $M_2 > 13 M_{\rm jup}$).

Pure ellipsodial variability produces a sinusoidal lightcurve, which is statistically consistent with Kelu-1's folded lightcurve. If a secondary companion is responsible for the variability, future observations will return the same amplitude and ephemeris. We note that a binary system would have an orbital velocity of $\sim 130 {\rm kms}^{-1}$, and would be capable of mimicing the observed $60 {\rm kms}^{-1}$ line broadening over a 1 hour integration.

4.4 Surface structures

Doppler imaging codes have been used extremely successful to mapping and understand the surface features on solar-type low-mass stars. However, the process requires very high quality photometry and spectroscopy, combined with a full understanding of photospheric physics; all of which seem a long way off for brown dwarfs.

Although mapping the surface of a brown dwarf is a distant goal, we can make some headway. By synthesising photometry from theoretical spectra (Allard et al. 2001) of two limiting cases; 1) dust is suspended in the atmosphere (*DUSTY*), and 2) dust forms, but immediately settles below the photosphere (*COND*), we can investigate what degree of surface structure is required to reproduce the observed variability.

Kelu-1's spectrum is best matched by a *DUSTY* atmospheric model (Baraffe et al. 1998), so we assume a model in which variability is caused by clear (*COND*) "holes" in a photosphere dominated by *DUSTY* "clouds". The *COND* spectrum is 0.55 mag brighter than the *DUSTY* spectrum through our filter. The amplitude of 0.012 mag we observe in Kelu-1 corresponds to *COND* "holes" covering $\sim$1.7% of an otherwise *DUSTY* photosphere. This value is a lower limit, as less perfect clear patches would have a smaller effect on the variability, requiring them to cover larger fractions of the surface.

Note that the covering fractions above actually represent the *difference* in covering fraction between maximum and minimum light. They are therefore only representative of surface features on $\sim 180°$ scale. It may be that the surface has a far more significant small scale structure, which simply averages out over large regions.

4.5 The radius of Kelu-1

Interpreting the 1.8h variability as the rotation period allows us to make one of the first firm tests of brown dwarf evolutionary theory. Evolutionary models (e.g. Chabrier et al. 2000) predict that after $\sim$100Myr, brown dwarfs (independant of mass) reach a stable radius of $\sim 0.1 R_\odot$. We can combine the rotation period and the rotational velocity to produce an observational lower limit (due to the unknown inclination) on Kelu-1's radius. For the observed values of 1.80$\pm$0.04h and 60$\pm$5kms^{-1} (Basri et al. 2000), Kelu-1 must have $R \geq 0.09 \pm 0.01 R_\odot$. The evolutionary models are therefore in agreement with our observations of Kelu-1. This is not the case for the observations of BRI0021-0214 made by Martín et al. (2001). They require a radius of at least $0.14 R_\odot$ to fit their observations with meta-stable photospheric surface features. We note that this argument would require the features responsible for photometric varibility to have the same rotation period as the photosphere.

Alternatively, we can invert this argument and, assuming a model radius of $0.1 \pm 0.05 R_\odot$ (to include a range of possible ages and masses), determine Kelu-1's inclination to the line of sight as $53 \leq i \leq 77$. This means that between 80% and 97% of the surface can cause variability. The remaining fraction (polar regions) is either permanently in view, or never visible.

5 CONCLUSIONS

It is now clear that variability from brown dwarfs can be detected, but that photometry of better than 1% is required to do so. In the near future, futher studies of variability and rotation in brown dwarfs should greatly increase our understanding of their physics.

We have detected a strong periodicity of 1.80$\pm$0.05 hours in differential photometry of the L2 brown dwarf Kelu-1. We have investigated four possible mechanisms to explain this variability:

(i) surface inhomogeneity moderated by meteorology and variable dust formation;
(ii) surface inhomogeneity moderated by magnetic starspots;
(iii) light curve variability due to gravitational distortion of Kelu-1's envelope by a close companion; and
(iv) light curve variability due to an eclipsing binary

Mechanisms (ii) & (iv) seem unlikely explanations, but we are unable to concusively differentiate between mechanisms (i) & (iii). Ellipsodial variability, mechanism (iii), would produce a twin peaked lightcurve, giving a period of 3.6$\pm$0.1 hours. This mechanism will give stable and repeatable photometric variability in future epochs. Alternatively, mechanism (i) associates the 1.80$\pm$0.05 hour period with the rotation period, which is consistent with the rotational

velocity of 60 kms^{-1} and theoretical radius of $\sim$0.1R$_\odot$, indicating an inclination in the range $53^\circ \leq i \leq 77^\circ$.

Over the duration of our observations, the general shape and period of the lightcurve are unchanged (at least to within the measurement noise), implying the process causing the modulations is also stable on this timescale. This is in contrast to previous variability observations where no periodicity, or a period that changes on the order of the observation length, has been measured.

The two explanations we have presented lead to different predictions for future observations of Kelu-1. Variability induced by a secondary companion will be completely repeatable at future epochs, whereas long term evolution of surface features will result in a secular changes in the lightcurve. Further observations of Kelu-1 will be a powerful discriminant between the two hypotheses we have presented.

6 ACKNOWLEDGEMENTS

We would like to thank the referee France Allard for her speedy reponse and very helpful comments. This paper is based on observations made at Anglo-Australian Telescope, Siding Spring, Australia. FJC acknowledges the support of a PPARC studentship award during the course of this research.

REFERENCES

Allard F., Hauschildt P. H., Alexander D. R., Tamani A., Schweitzer A., 2001, ApJ, 556, 357
Basri G., Mohanty S., Allard F., Hauschildt P. H., Delfosse X., Martín E. L., Forveille T., Goldman B., 2000, ApJ, 538, 363
Bailer-Jones C. A. L., Mundt R., 1999, 348, 800
Bailer-Jones C. A. L., Mundt, R., 2001, A&A, 367, 218
Baraffe I., Chabrier G., Allard F., Hauschildt P., 1998, A&A, 337, 403
Chabrier G., Baraffe I., Allard F., Hauschildt, P., 2000, ApJ, 542, 464
Frandsen S., Jones A., Kjeldsen H., Viskum M., Hjorth J., Andersen N. H., Thomsen, B., 1995, A&A, 301, 123
Gelino C. R., Marley M. S., Holtzman J. A., Ackerman A. S., Lodders K., 2001, ApJL, submitted
Hilditch R. W., 2001, An Introduction to Close Binary Stars, C.U.P, Cambridge
Kirkpatrick J. D., Allard F., Bida T., Zuckerman B., Becklin E. E., Chabrier G., Baraffe I., 1999, ApJ, 519, 834
Kirkpatrick J. D. et al., 2000, AJ, 120, 447
Martín E. L., Delfosse X., Basri G., Goldman B., Forveille T., & Zapatero Osorio M. R., 1999, AJ, 118, 2466
Martín E. L., Zapatero Osorio M. R. & Lehto H. J., 2001, ApJ, 557, 822.
Roberts D.H., Lehar J., Dreher J.W., 1987, AJ, 93, 968.
Ruiz M. T., Leggett S. K., Allard F., 1997, ApJL, 491, L107
Schubert G., Zhang K., 2000, ASP conf 212, 210
Stauffer J. B., Hartmann L. W., 1986, PASP, 98, 1233
Tinney C. G., 1998, MNRAS, 296, L42
Tinney C. G., Reid I. N., 1998, MNRAS, 301, 1031
Tinney C. G., Tolley, A. J., 1999, MNRAS, 304, 119